Ultrasound in Med. & Biol., Vol. 39, No. 4, pp. 681–691, 2013

0301-5629/$ - see front matter

http://dx.doi.org/10.1016/j.ultrasmedbio.2012.10.019

● *Original Contribution*

SUPPRESSION OF GRATING LOBE ARTIFACTS IN ULTRASOUND IMAGES FORMED FROM DIVERGING TRANSMITTING BEAMS BY MODULATION OF RECEIVING BEAMS

AKINLOLU PONNLE,* HIDEYUKI HASEGAWA,*† and HIROSHI KANAI*†

*Graduate School of Engineering, Tohoku University, Sendai, Japan; and †Graduate School of Biomedical Engineering, Tohoku University, Sendai, Japan

(*Received* 20 *October* 2011; *revised* 22 *October* 2012; *in final form* 30 *October* 2012)

Abstract—In linear array transducers, owing to regular spacing of the array elements, grating lobes exist in transmission and reception. In ultrasonic imaging involving the use of diverging (unfocused) transmitting beams and steered receiving beams by linear transducer arrays, aperture apodization and spatial combination of steered receiving beams from multiple transmissions are not sufficient to suppress receive-grating lobe artifacts. To further suppress receive-grating lobe artifacts in reconstructed B-mode images, we propose a technique of modulating the receiving beams by a factor that is governed by the envelope of a corresponding signal, which is formed by filtering the receiving beam with a zero-phase low-pass filter with a cut-off frequency that is determined by the receiving beam steering angle. This technique suppressed receive-grating lobe artifacts without significant loss in spatial resolution in offline reconstructed B-mode images from simulation, phantom and *in vivo* imaging of the carotid artery. In a simulation of point scatterers, a relative reduction in grating lobe artifacts of 40 dB was realized in images from diverging beam scanning. (E-mail: ponnleakinlolu@yahoo.co.uk) © **2013 World Federation for Ultrasound in Medicine & Biology.**

Key Words: **Receive-grating lobe, Diverging transmitting beam, Zero-phase low-pass filter, Bidirectional filtering, Modulated receiving beam.**

INTRODUCTION

In linear array transducers, owing to regular spacing of the array elements, grating lobes exist in transmission and reception if the inter-element pitch is wider than a wavelength (Barthez et al. 1997; De Jong et al. 1985; Kremkau 2006; Kremkau and Taylor 1986). The receive-grating lobe angle depends on the steering angle of the main receiving lobe, inter-element pitch and the wavelength. In applications in which an unfocused, wide beam is transmitted—such as in synthetic aperture imaging, parallel receive beam forming (Jensen et al. 2006; O'Donnell 1990; Thomson 1984), explososcan, ultrafast ultrasound imaging (Delannoy et al. 1979; Fink et al. 2002; Shattuck et al. 1984), or multi-element diverging transmission beam scanning (Ponnle et al. 2011)—the effect of receive-grating lobes is significant because of the reception of echoes from several directions that the transmission beam insonifies. These backscattered echoes may contain signals of different frequency components when pulsed ultrasound is used for imaging. Because the receive-grating lobe angle varies with the frequency of the incoming signals, a receiving beam formed for a given direction may have a wide frequency spectrum containing echo signals from the desired direction as well as directions of the grating lobes. Although grating lobe intensity can be reduced by apodization (De Jong et al. 1985) and by combining receiving beams from multiple transmissions (Ponnle et al. 2011), these measures are not sufficient.

A method of adjustable frequency scanning to reduce grating lobe artifacts in scanning a field of view using a scan format has been described previously by Wright et al. (1996; U.S. Patent No. 5549111). In this patent, the carrier frequency of the imaging pulse transmitted into the body is highest in the center portion of the scan and is reduced in a controlled fashion as the steering angle is increased without modification of the pulse shape itself. This arrangement permits a combination of

Address correspondence to: Akinlolu Ponnle, Department of Electronic Engineering, Graduate School of Engineering, Tohoku University, 6-6-05 Aramaki-aza-Aoba, Aoba-ku, Sendai 980-8579, Japan. E-mail: ponnleakinlolu@yahoo.co.uk

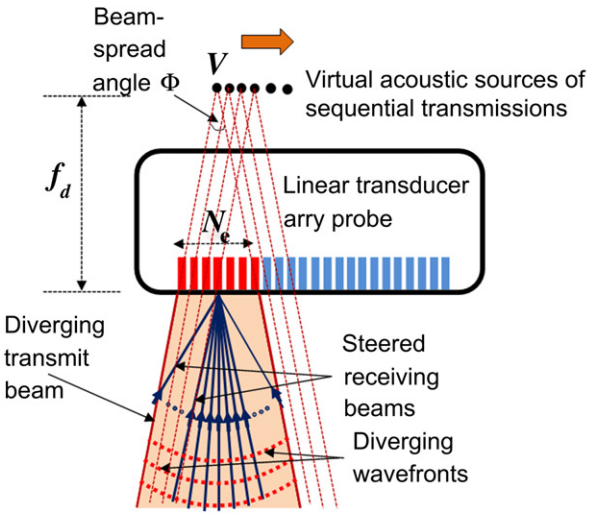

Fig. 1. Illustration of the transmission and reception scheme of the multi-element diverging beam scanning from a linear array transducer.

high-frequency imaging operation (high resolution) in the central portion of the image with a wide field of view that suppresses grating lobe artifacts in the outer portions of the image, but with reduced lateral resolution.

A means of reducing the grating lobe by decreasing the imaging frequency on a scan-line–by–scan-line basis was described by Yamaguchi et al. (1986; U.S. Patent No. 4631710). In this patent, a variable bandpass filter (containing a wideband amplifier, a variable high-pass filter and a variable low-pass filter) is described whose characteristics are controlled as a function of steering angle. As described, the filter can be applied to a combination of each output from a pulse or transmitter, each reception signal from a receiving transducer element, a composite receiving beam and original transmission or excitation signal. Providing one such device per transmission channel and/or one per receive channel is prohibitively complex and electronic component intensive. The approach also suffers from an inherent loss of signal-to-noise ratio because useful energy is lost.

Using angular compounding for strain imaging, Hansen et al. (2006) applied low-pass filtering to the receive-beam–formed radiofrequency (RF) signals after transmitting conventional focused beams at large steering angles from a linear transducer array to reduce grating lobe artifacts, but at the cost of spatial resolution.

In this work, a wide multi-element diverging (unfocused) transmitting beam from a linear array transducer with scanning in a linear sequential fashion (across the array) was used. The ultrasonic RF echo data received by the elements in the receiving sub-aperture within each transmitting event are used for offline creation of many steered receiving beams at regular angular intervals. The maximum steering angle of receiving beams in each transmission beam is limited to ±65 degrees with an inter-beam angular separation of 0.5 degrees. The steered receiving beams were then processed further, and a B-mode image was reconstructed from combinations of many steered receiving beams from multiple transmissions per frame.The transmission and reception principle is illustrated in Figure 1. In the figure, each point V is the virtual acoustic (point) source behind the actual array surface (Gammelmark and Jensen 2003; Karaman et al. 1995; Lockwood et al. 1998; Nikolov et al. 1999); f_d is the axial distance from the array surface to the virtual acoustic source V; Φ is the beam-spread angle; and N_e is the number of active elements that compose the transmitting sub-aperture.

To further suppress receive-grating lobe artifacts in offline-reconstructed B-mode images from diverging transmission beam scanning, we proposed a method of modulating each steered receiving beam by a varying factor governed by the envelope of a corresponding signal, which was formed by filtering the receiving beam through a zero-phase (ZP) low-pass filter (LPF) with a cut-off frequency dependent on the main receiving beam steering angle. The receiving beams are modulated rather than using the low-pass–filtered signals to keep the phase information of the receiving beams unaffected and to preserve the spatial resolution of the reconstructed image.

Reconstructed B-mode images from simulated scanning of point scatterers in water and from scanning of the transverse cross-section of a silicone-rubber tube phantom in water, as well as *in vivo* scanning of carotid artery, show that receive-grating lobe artifacts are significantly suppressed in the images in which the proposed technique was applied without a loss of spatial resolution.

Principle

For a linear array transducer, the location (angle θ_g) of receive grating lobes is obtained as (Huang et al. 2004):

$$\theta_g = \sin^{-1}\left(\sin\theta_s - \frac{m\lambda}{p}\right), \quad (\mathrm{m} = \pm 1,\ \pm 2,\ \pm 3,\ \ldots) \tag{1}$$

where p is the inter-element pitch, λ is the receive-signal wavelength, θ_s is the steering angle of the main receiving lobe and m is a signed integer that is the order of the grating lobes. The location of the main receiving lobe corresponds to the value of $m = 0$.

Considering the first order grating lobe ($m = \pm 1$),

$$\theta_g = \sin^{-1}\left(\sin\theta_s \pm \frac{\lambda}{p}\right). \tag{2}$$

Because λ is real,

$$\lambda = p\left(\sin|\theta_g| + \sin|\theta_s|\right) = \frac{c_o}{f}, \tag{3}$$

where c_o is the speed of ultrasound in the medium.

Therefore, the receive-grating lobe angle θ_g, the receiving beam steering angle θ_s, and the inter-element pitch p are related to the receive-signal frequency f by:

$$f = \frac{c_o}{p\left(\sin|\theta_g| + \sin|\theta_s|\right)} \tag{4}$$

Considering a receiving beam at steering angle θ_s, as θ_g increases (from 0 degrees), f decreases until $\theta_g = 90$ degrees at $f = f_c$ (cut-off frequency). This implies that at frequencies $>f_c$, grating lobes exist at different angles between 0 and 90 degrees. This finding is illustrated in Figure 2 for a main receiving beam at 0 degrees, having different directions of first-order receive-grating lobes, θ_g at different frequencies.

Cut-off frequency

At the cut-off frequency, the grating lobe angle is 90 degrees. Substituting 90 degrees for θ_g in eqn (4), the cut-off frequency f_c can be expressed as:

$$f_c = \frac{c_o}{p(1 + \sin|\theta_s|)} \tag{5}$$

Given a steering angle θ_s, the cut-off frequency can be determined. It should be noted that in this approach, the center frequency of the transmitted pulse is constant, but the steered receiving beams formed in each transmitting event are low-pass filtered with different cut-off frequencies determined by the respective receiving beam steering angles. There could be a large overlap in the frequency range between the grating lobes at various angles because there are multiple cut-off frequencies and receiving beam steering angles are different.

Zero-phase low-pass filtering by bidirectional recursive filtering

A ZP filter is a non-causal filter that can be used on a finite sequence of signal data. It is a special filter in which the slope of the phase response with frequency is zero. It is possible to implement a ZP filter offline by using a recursive infinite impulse response (IIR) filter in bidirectional filtering operation; this squares the amplitude response and zeros the phase response (Gustafsson 1996; Smith 1997). It is desirable that the LPF have as maximally flat a magnitude frequency response as possible in the passband and stopband, as well as a steep frequency roll-off toward zero in the transition band.

In this work, ZP filtering was performed by first designing a seventh-order Butterworth (IIR) LPF (Selesnick and Burrus 1996; Shenoi 2006; Shenoi and Agrawal 1980) with cut-off frequencies as determined by eqn (5). The designed filter was then used on the receiving beam data in a bidirectional recursive filtering operation to cancel out the phase shifts.

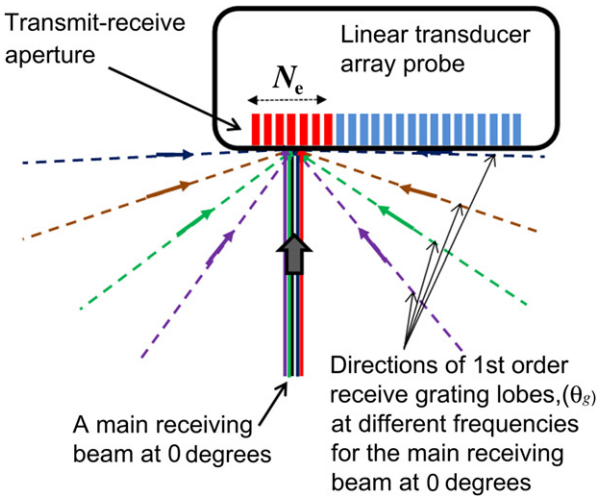

Fig. 2. Illustration of a main receiving beam (at 0 degrees) and associated different first-order receive-grating lobe angles (θ_g) at different frequencies.

The impulse response of the seventh-order Butterworth (IIR) LPF (at a cut-off frequency of 7.5 MHz and a sampling frequency of 40 MHz) with and without the ZP operation is shown in Figure 3 (a, b) and the corresponding frequency magnitude/phase responses are shown in Figure 3 (c, d). In Figure 3b, the ZP-LPF removes the time shift and makes the impulse response symmetrical in time, though only positive time samples are shown. Also in Figure 3d, it can be observed that while the phase varies non-linearly with frequency for the IIR filter, the resulting phase shift by the ZP-LPF is maintained at almost zero throughout the pass band.

Proposed modulating technique

To keep the phase information of the receiving beams unaffected and to preserve the spatial resolution of the reconstructed image, the receiving beams are modulated rather than using the LPF signals for image reconstruction. The receiving beams are modulated indirectly by the output of the ZP-LPF according to the proposed technique shown in Figure 4. The modulating signal $R_F(n,\theta)$ is obtained by operation A1 defined by:

$$R_F(n,\theta) = \begin{cases} \dfrac{y_{f(env)}(n,\theta)}{y_{env}(n,\theta)} & \text{if } y_{f(env)}(n,\theta) < y_{env}(n,\theta) \\ 1 & \text{otherwise} \end{cases} \tag{6}$$

where $y_{env}(n,\theta)$ is the envelope of the original receiving beam signal $y(n,\theta)$, and $y_{f(env)}(n,\theta)$ is the envelope of the

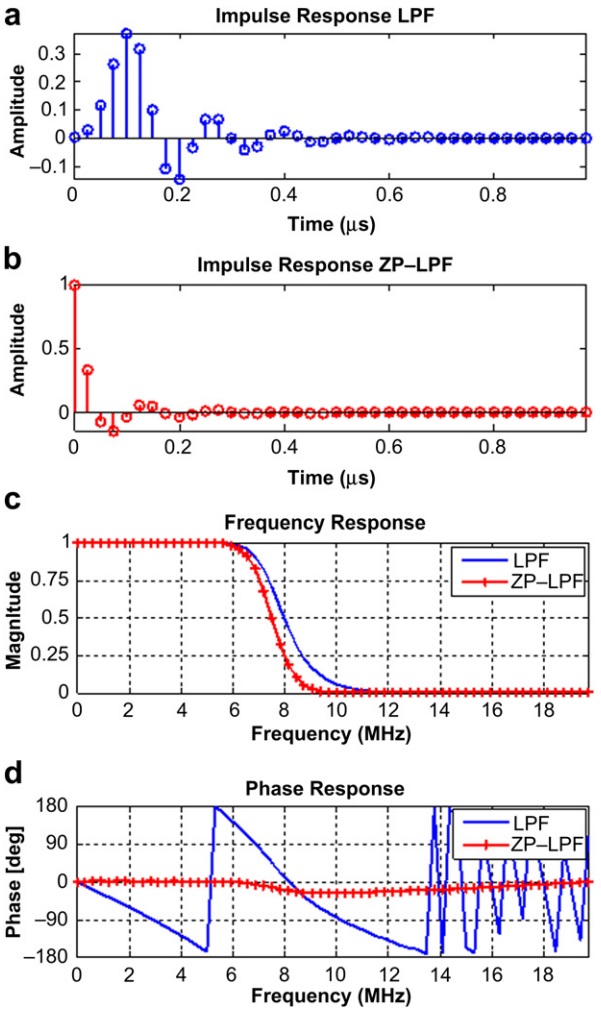

Fig. 3. Characteristics of the seventh-order Butterworth (IIR) low-pass filter (cut-off frequency of 7.5 MHz at sampling frequency of 40 MHz): (a) Impulse response without zero phase operation, (b) Impulse response with zero phase operation, (c) frequency response, (d) phase response.

ZP-LPF signal $y_f(n,\theta)$. The output signal $y_m(n,\theta)$ is the modulated receiving beam signal given by

$$y_m(n,\theta) = R_F(n,\theta) \times y(n,\theta) \tag{7}$$

where θ is the beam steering angle.

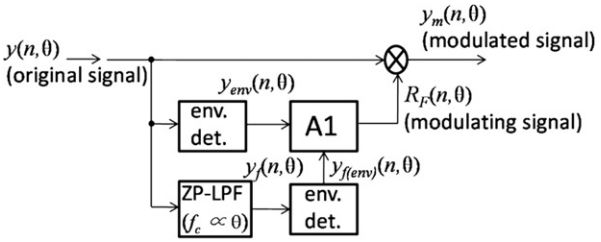

Fig. 4. Proposed modulating technique. env. det. = envelope detection.

Operation A1 as defined by eqn (6) allows for modulation of the receiving beams without affecting the resolution of the final B-mode image. In addition, the series of modulating weights could be represented as a direct current (d.c.) signal with some arbitrary alternating current (a.c.) signals riding on it. Therefore, the multiplication shows that the overall bandwidth of the modulated receiving beams is still comparable to the frequency band of the original receiving beam, but the peaks and troughs in the spectra are slightly modified.

The modulating signal $R_F(n,\theta)$ as determined by operation A1, when multiplied with the original receiving beam $y(n,\theta)$, brings down the average amplitude level of $y(n,\theta)$ close to that of the ZP-LPF signal for comparison; it also ensures that $y(n,\theta)$ is not completely modulated by the entire ZP-LPF envelope. Comparing the ZP-LPF signal with the original receiving beam signal, the amplitude of the receive-grating lobe and depth side-lobe signals in the ZP-LPF signal would be relatively reduced. Therefore, the proposed modulating technique attempts to modify the amplitude variations of the original receiving beam signal $y(n,\theta)$ to follow the amplitude variations of the ZP-LPF signal in time portions of the original signal, in which the amplitude of the ZP-LPF signal is less than the amplitude of the original signal, while retaining the level of the original signal in time portions in which the amplitude of the ZP-LPF signal is greater. This technique prevents the spreading effect of the envelope of the ZP-LPF signal in the depth direction from affecting the modulated receiving beam signal $y_m(n,\theta)$.

The offline creation of steered receiving beams, synthesis of the IIR LPF, bidirectional filtering, beam modulation and image reconstruction were all performed using MATLAB software (MathWorks, Natick, MA, USA).

MATERIALS AND METHODS

Simulations

Three columns of six point-scatterers of equal strength—separated by a lateral distance of 14 mm with each point-scatterer in each column positioned at axial depths of 10, 12, 14, 16, 18 and 20 mm in water—were simulated, and virtual (simulated) diverging transmitting beam scanning at a beam-spread angle Φ of 90 degrees with a simulated 192-element linear array transducer was performed using Field II program developed by Jensen (Jensen 1996). A transmitting sub-aperture of 36 elements was used, thereby making 157 transmissions per frame possible. The scatterers were positioned, and the columns were distanced apart to enable visualization of the grating lobe artifacts of the point-scatterers and how much they affect (*i.e.,* blur) the image of the

Table 1. Parameters for the virtual (simulated) scanning of point-scatterers in water

Parameter	Value
Transmitting frequency (MHz)	7.5
Sampling frequency (MHz)	30
Transmitting sub-aperture size (elements)	36
Assumed speed of sound in water (m/s)	1500
Assumed attenuation in water (dB/cm)	0
Transmitting and receiving apodization	Boxcar
Element excitation	Hanning-modulated sinusoid of 2 cycles
Interval of centers of transmitting sub-apertures (mm)	0.2 (one-element pitch)
Beam-spread angle (degrees)	90
Virtual source point for the diverging beam	3.5 mm behind the array surface

point-scatterers. The position of each column of scatterers, especially the central column, fell within the region where the grating lobe artifacts of the point scatterers of other columns were prominent. Other simulation parameters are shown in Table 1.

Silicone-rubber tube phantom scanning

A silicone-rubber tube phantom in water was scanned in the transverse plane using diverging transmitting beams having a beam-spread angle Φ of 90 degrees; 36 elements as the transmitting sub-aperture and 96 elements as the receiving sub-aperture per transmission. Using a 192-element linear array transducer having

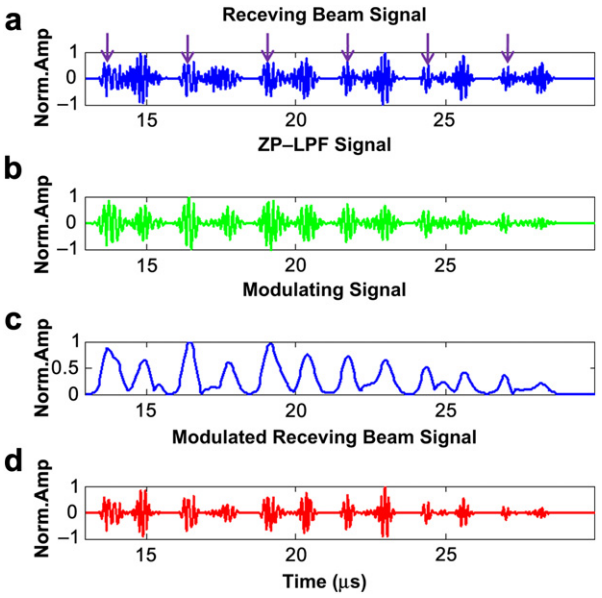

Fig. 5. Waveforms of the (a) receiving beam, (b) its zero-phase low-pass filtered signal, (c) the modulating signal and (d) the modulated receiving beam for 0 degrees receive-steering angle for the 79th transmission of 157 transmissions per frame (simulation). Norm.Amp. = Normalized amplitude.

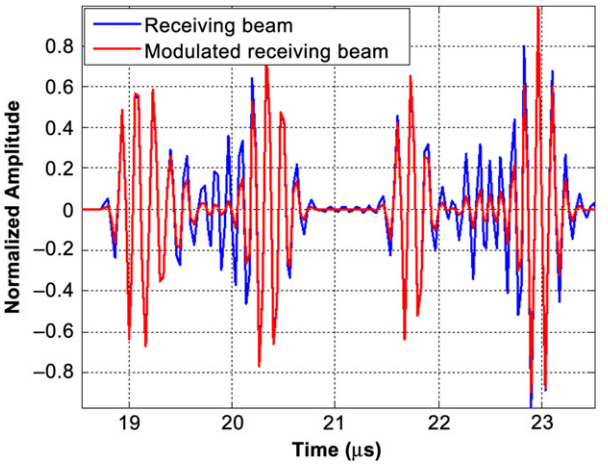

Fig. 6. Zoom-in portion of the receiving beam and the modulated receiving beam of Figure 5 (a, d) superimposed after normalization for comparison.

200-μm inter-element pitch (UST-5545, Aloka Co., Tokyo, Japan) with α-10 Aloka ultrasound equipment, 157 transmissions were made per frame, as done in the simulation. The received ultrasonic RF echoes of each element were acquired and sampled at a frequency of 40 MHz for offline processing and image reconstruction.

Carotid artery in vivo *scanning*

Transverse cross-sectional scanning of the carotid artery of three human subjects (adult men) was performed using diverging transmitting beams with the same transmission, array transducer, ultrasound equipment and data acquisition parameters used in the silicone-rubber tube phantom scanning.

RESULTS

Simulations

Figure 5 (a–d) shows the waveforms of the 0-degree steered receiving beam signal $y(n,\theta)$, the ZP-LP filtered signal $y_f(n,\theta)$, the modulating weight $R_F(n,\theta)$ and the modulated receiving beam signal $y_m(n,\theta)$ of the 79th transmission of the 157 transmissions per frame, $y(n,\theta)$ being created from the received RF signals of the receiving sub-aperture elements. This receiving beam coincides with the center column of the point scatterers. The positions of the point-scatterers are indicated by the arrows in Figure 5a. In Figure 5d (compared with Fig. 5a), the temporal lengths of signals due to grating lobes and lateral and depth side-lobes are reduced, but temporal lengths of signals from the point-scatterers are retained. This finding can also be observed in Figure 6, which is a zoom-in portion of the receiving beam and the modulated receiving beam signals of Figure 5 (a, d) superimposed after respective normalization for comparison. The two signals are still aligned in time, but the

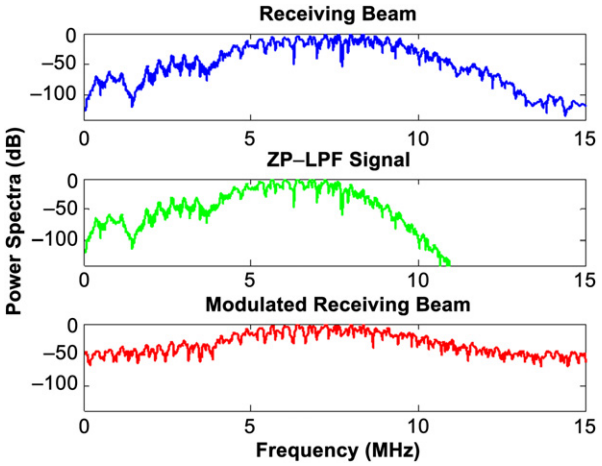

Fig. 7. Power spectra of the corresponding waveforms in Figure 5.

instantaneous amplitude of the modulated receiving beam is modified.

Figure 7 shows the power spectra of the signals in Figure 5 (a, b, d). The frequency band of the ZP-LPF signal is reduced because of the filtering (cut-off frequency is 7.5 MHz in this case), but the frequency band of the modulated receiving beam signal extends well beyond the cut-off frequency of the ZP-LPF signal. In addition, the overall frequency band of the modulated receiving beam is still comparable to the frequency band of the original receiving beam, although the peaks and troughs are modified because of the multiplication between the modulating weights and the original receiving beam signal, as shown by eqn (7).

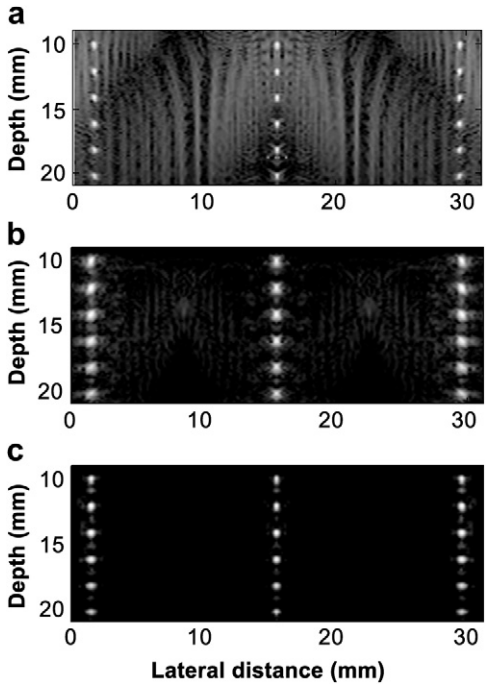

Fig. 8. Reconstructed B-mode image of simulated scanning of simulated point-scatterers using diverging beam scanning (a) from receiving beams, (b) from ZP-LPF signals and (c) from modulated receiving beams (images in 60 dB range).

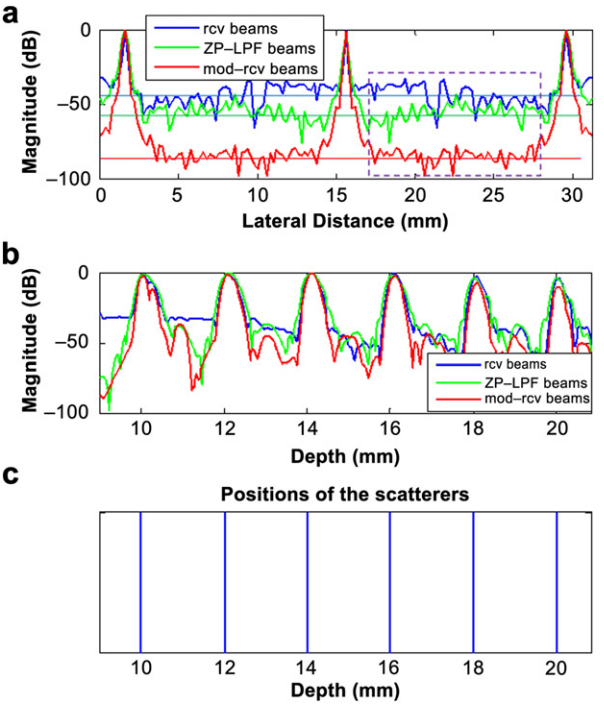

Fig. 9. (a) Lateral profile at a depth of 14 mm. (b) Depth profile along the scatterers of the central column. (c) Positions of the point-scatterers of (b).

Figure 8 (a–c) shows the reconstructed B-mode images of the simulated point-scatterers from the receiving beams, ZP-LPF signals and the modulated receiving beams, respectively. The images are reconstructed from 157 transmissions and a lateral distance >30 mm to visualize the grating-lobe artifacts of the point-scatterers, which are pronounced at the top edge of the image in Figure 8a. For reconstruction of the steered receiving beams, boxcar apodization was used. In Figure 8b, the artifacts are reduced but at the expense of loss in spatial resolution because of the LPF. In Figure 8c, the artifacts are suppressed without a loss in spatial resolution.

Figure 9a shows the lateral profile at a depth of 14 mm. Figure 9 (b, c) shows the depth profile along the point-scatterers of the central column and the positions of the scatterers. As can be seen in Figures 8 and 9a, the lateral profiles of the point-scatterers in the ZP-LPF image are wider, whereas those using the proposed technique are still comparable to the image from the original receiving beams. In addition, the lateral side-lobes (Fig. 9a) and the depth side-lobes (Fig. 9b) are significantly reduced. The depth side-lobes are caused by the

Table 2. Half-maximum width and relative change in half-maximum width of image of the point-scatterer at a depth of 14 mm along the central column of scatterers

	Half-maximum width (mm)			Relative change in half-maximum width, X (%)	
	Receiving beams	ZP-LPF signals	Modulated receiving beams	Receiving beams: ZP-LPF signals	Receiving beams: mod-receiving beams
Lateral	0.212	0.238	0.225	−12.2	−6.1
Axial	0.295	0.365	0.267	−23.7	9.5

ZP-LPF = zero-phase low-pass filter.

trailing pulses, which propagate after the main pulses of the wavefronts of the diverging transmitting beam (Ponnle et al. 2011). The main pulses are the effective pulses for imaging.

Suppression of grating lobe artifacts

Considering the lateral profile plots of Figure 9a, the lateral region considered for evaluation of the suppression of grating lobe artifacts is shown enclosed by the broken purple line. Within these regions, the average level of the image signal for each case is indicated by the horizontal line of corresponding color running across the regions. The image signals within these regions are the result of the combined effect of side-lobes and grating-lobe artifacts of the scatterers. The average levels of image signals are −43.7, −56.2 and −83.3 dB for the image from receiving beams, ZP-LPF signals and modulated receiving beams, respectively. Regarding the image from the receiving beams, these values indicate a reduction of 12.5 dB by the ZP-LPF signals and a reduction of ∼40 dB by the modulated receiving beams.

Half-maximum width of image of point scatterer and resolution

The effect on image point spread (resolution) is evaluated as:

$$X = \frac{a-b}{a} \tag{8}$$

where a is the half-maximum width of the image point spread from receiving beams, b is the half-maximum width of the image point spread from other cases (ZP-LPF and modulated receiving beams) and X indicates relative change in the image point spread. The half-maximum widths with corresponding values of X (in percentage) were evaluated for the point scatterer at 14 mm in depth in the central column from Figure 9, as summarized in Table 2. A positive value for X indicates improvement, whereas a negative value for X indicates otherwise.

For the diverging beam scanning, there is a significant loss in both axial and lateral resolution by the ZP-LPF signals. This loss is not unexpected because in the image formation from the diverging beam scanning, several steered receiving beams are spatially combined, and filtering is performed in the direction of steering of the receiving beams. Therefore, this would degrade the resolution both laterally and axially.

However, using the modulated receiving beams, a slight loss of lateral resolution is noticed in Table 2, but there is an improvement in resolution along the depth by suppression of the depth side-lobes. The loss in lateral resolution is marginal and does not have much effect on the B-mode image. It should be noted that these analyses are from images produced by simulations.

Phantom

Figure 10 (a–c) shows the reconstructed B-mode images obtained from the scanning of the silicone-rubber tube phantom in water from the receiving beams, ZP-LPF signals and the modulated receiving beams, respectively. The images are reconstructed from 157 transmissions and over a lateral distance >30 mm to observe the grating lobe artifacts due to the wall of the phantom, which is conspicuous at the edges of the image in Figure 10a. As is the case in the simulation, grating lobe artifacts are suppressed in Figure 10b, but the spatial resolution is degraded because of the LPF. Using the proposed modulation method, grating lobe artifacts are significantly reduced in Figure 10c without a loss in spatial resolution.

Figure 10d shows the axial (depth) profile along the center of the tube for the B-mode image from receiving beams, ZP-LPF signals and the modulated receiving beams, respectively. As shown in the figure, the level of depth side-lobes in the image from the ZP-LPF signals and the modulated receiving beams are more reduced than in the image from the receiving beams. In addition, in the depth profile, there is a loss in spatial resolution of the image from the ZP-LPF signals (the thickness of the tube's wall is wider for the ZP-LPF signals), but no significant loss in spatial resolution for the modulated receiving beams (same thickness of tube's wall as that of the receiving beams).

As stated earlier, the grating lobe artifacts caused by the wall of the tube are more pronounced (and the suppression resulting from the proposed technique is more observed) toward the edges of the image in

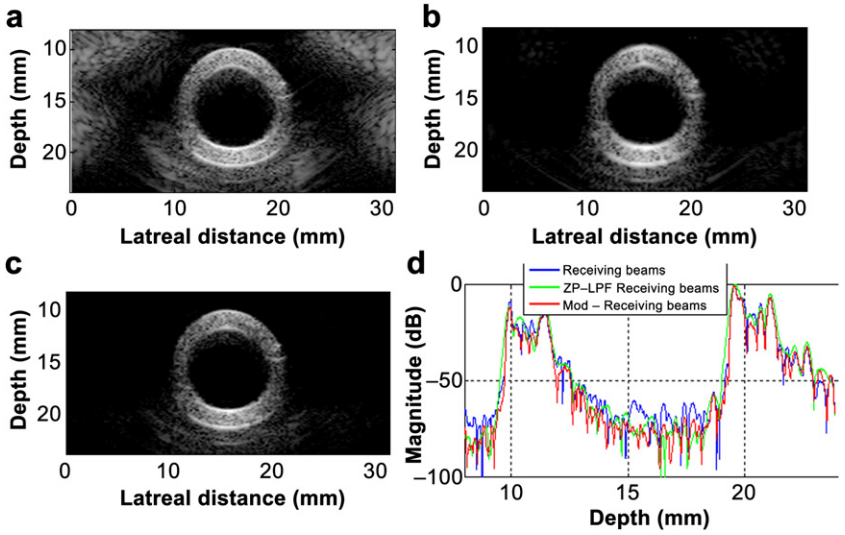

Fig. 10. Reconstructed B-mode images of the silicone-rubber tube phantom in the transverse cross-sectional plane from (a) receiving beams, (b) ZP-LPF signals and (c) modulated receiving beams (images in 60 dB range).(d) Depth profile along the center of the tube in the B-mode image in (a), (b) and (c).

Figure 10a; therefore, few observed grating lobe artifacts are present at the center of the image, where the depth profile is taken.

In vivo *imaging*

For scanning of the carotid artery, Figure 11 (a–c) shows the reconstructed B-mode images obtained from the receiving beams, ZP-LPF signals and the modulated receiving beams, respectively. Comparing the three *in vivo* images, the images in Figure 11 (b, c) are clearer than in Figure 11a. In Figure 11b, although receive-grating lobe artifacts are reduced, there is a degradation of spatial resolution. In Figure 11c, receive-grating lobe artifacts are significantly suppressed without degradation of the spatial resolution. Some image features blurred by receive-grating lobe artifacts in Figure 11a can be seen clearly in Figure 11c. In addition, image contrast is enhanced.

For the scanning of the carotid artery of the other two subjects, Figures 12 (a–c) and 13 (a–c) show reconstructed B-mode images obtained from the receiving beams, ZP-LPF signals and the modulated receiving beams.

DISCUSSION

Aperture apodization can reduce side-lobes and grating lobes to some extent, but it also widens the main lobe, which reduces the spatial resolution. In this

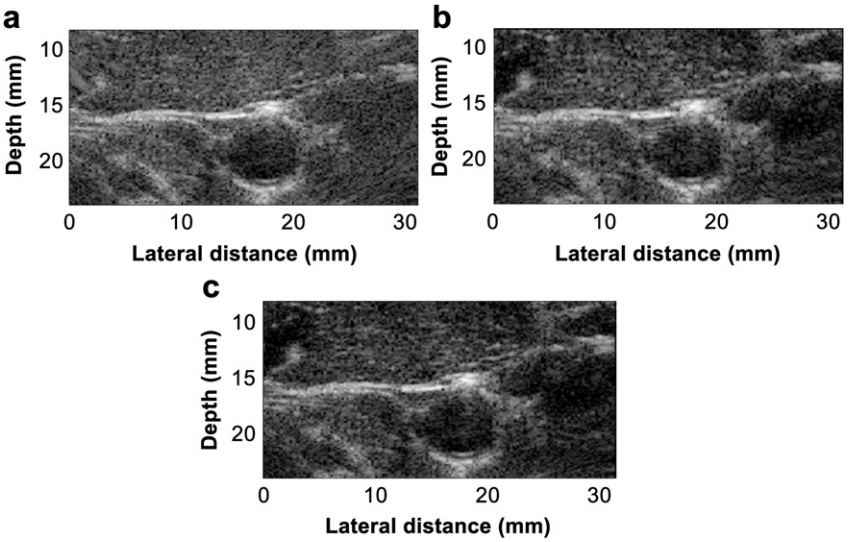

Fig. 11. Reconstructed B-mode images of the carotid artery of the first subject in the transverse cross-sectional plane from (a) receiving beams, (b) ZP-LPF signals and (c) modulated receiving beams (images in 60 dB range).

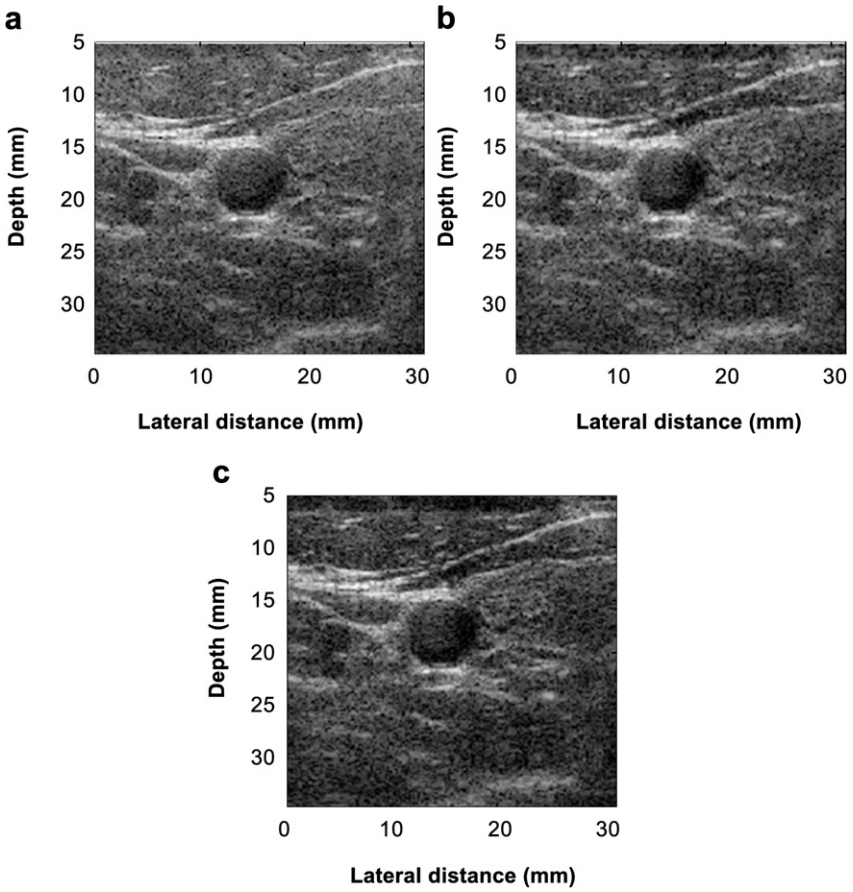

Fig. 12. Reconstructed B-mode images of the carotid artery of the second subject in transverse cross-sectional plane from (a) receiving beams, (b) ZP-LPF signals and (c) modulated receiving beams (images in 60 dB range).

work, boxcar aperture apodization was used in the creation of the steered receiving beams to have a narrow main receiving lobe.

Spatial combination of steered receiving beams from multiple transmissions also reduces grating-lobe artifacts because the grating lobe components in each receiving beam that are spatially combined at an image point will not be coherent. If there is a sufficient number of steered receiving beams (positive-angled and negative-angled receiving beams) that are combined at an image point, grating lobe artifacts are reduced significantly. However, in parts of the image region where there is considerable imbalance in the number of the positive-angled and negative-angled receiving beams that are spatially combined, the incoherent grating lobe components in each receiving beam might not be completely cancelled out by the combination; therefore, artifacts will appear in such regions in the image. These regions will be close to the edge of images corresponding to the regions of transmitting beams of the few initial transmissions and regions of transmitting beams of the few final transmissions in a frame (assuming linear sequential scanning).

Using the method proposed herein, this phenomenon will no longer have an effect, because in every steered receiving beam that is spatially combined, the amplitudes of the grating lobe components have already been reduced. For single-angle conventional scanning and images, grating lobe artifacts are stretched more for lower frequencies than for higher frequencies (Hansen et al. 2009). In this method, the grating lobe artifacts resulting from each steered receiving beam are stretched beyond the surface of the transducer by the filtering operation before combination.

By modulating the receiving beam signals using the proposed technique described in this article, the proposed method can not only compensate for some loss in spatial resolution, but it can also further suppress grating lobe artifacts as can be observed in images from the simulation, tube scanning and the *in vivo* scanning. Grating lobe generating signals are not only suppressed, but so are some non-grating lobe-generating signals that might carry useful clinical information. Nevertheless, the proposed modulation technique (which is to prevent loss in spatial resolution) involves only operations with signal envelopes; therefore, ZP filtering is required to

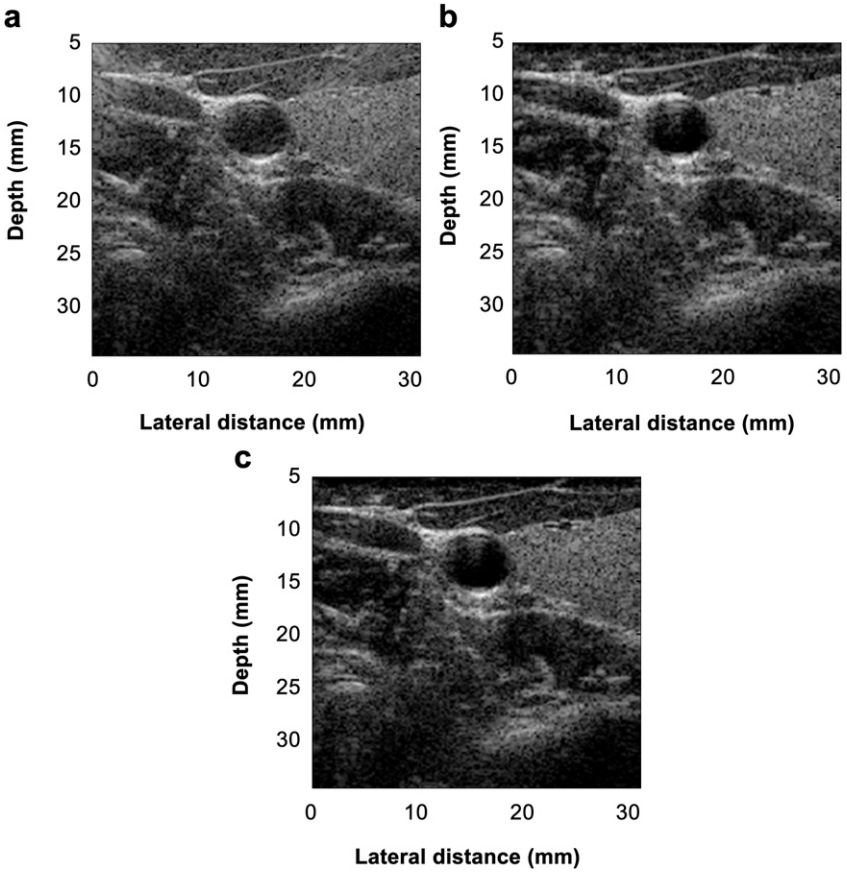

Fig. 13. Reconstructed B-mode images of the carotid artery of the third subject in the transverse cross-sectional plane from (a) receiving beams, (b) ZP-LPF signals and (c) modulated receiving beams (images in 60 dB range).

prevent relative time shifts between the original receiving beams and the LPF signals.

CONCLUSION

In ultrasonic imaging using diverging transmitting beams and steered receiving beams, although the spatial combination of steered receiving beams from multiple transmissions reduces the problem of receive grating lobes, the proposed method in this study further suppressed receive grating-lobe artifacts. Reduction of ~40 dB in the level of grating-lobe artifacts was achieved in simulations.

The modulating technique used in this work is effective for keeping the phases of the steered receiving beams unaffected and for preserving the spatial resolution of the reconstructed image.

Although the image produced from diverging beam scanning seems to be more prone to grating-lobe artifacts, diverging beam scanning has the advantage of obtaining images that are better than those of conventional linear scanning in terms of angular features that become more clearly visible at frame rates still comparable to conventional linear scanning. The diverging beam, as used in this work, requires no steering of transmitting beams but the steering was performed in reception. Diverging beam scanning is more suitable for imaging of the transverse cross section of circular structures.

Acknowledgments—This study was partly supported by a Grant-in-Aid for Research from Japan Society for the Promotion of Science (2011-2013, No. 23360177).The study was approved by the Ethics Committee on Clinical Investigation, Graduate School of Engineering, Tohoku University, and was performed in accordance with the policy of the World Medical Association Declaration of Helsinki Ethical Principles for Medical Research involving Human Subjects. All subjects gave informed consent.

REFERENCES

Barthez PY, Leveille R, Scrivani PV. Sidelobes and grating lobe artifacts in ultrasound images. Vet Radiol Ultrasound 1997;38:387–393.

De Jong N, Souquet J, Faber G, Bom N. Transducers in medical ultrasound: Part two. Vibration modes, matching layers and grating lobes. Ultrasonics 1985;23:176–182.

Delannoy B, Torquet R, Bruneel C, Bridoux E, Rouvaen JM, Lasota H. Acoustical image reconstruction in parallel processing analog electronic systems. J Appl Phys 1979;50:3153–3159.

Fink M, Sandrin L, Tanter M, Catheline S, Chaffai S, Bercoff J, Gennisson JL. Ultra High Speed Imaging of Elasticity. Proc IEEE UltrasonSymp 2002;2:1811–1820.

Gammelmark K, Jensen JA. Multi-element synthetic transmit aperture imaging using temporal encoding. IEEE Trans Med Imaging 2003;22:552–563.

Gustafsson F. Determining the initial states in forward-backward filtering. IEEE Trans Signal Process 1996;44:988–992.

Hansen HHG, Lopata RGP, De Korte CL. Non-invasive carotid strain imaging using angular compounding at large beam spread angles: Validation in vessel phantoms. IEEE Trans Med Imaging 2009;28: 872–880.

Huang J, Que PW, Jim JH. A parametric study of beam steering for ultrasonic linear phased array transducer. Russ J Nondestr Test 2004;40: 254–259.

Jensen JA. Field: A program for simulating ultrasound systems. Med Biol Eng Comput 1996;34:351–353.

Jensen JA, Nikolov SI, Gammelmark KL, Pedersen MH. Synthetic aperture ultrasound imaging. Ultrasonics 2006;44:e5–e15.

Karaman M, Li P, O'Donnell M. Synthetic aperture imaging for small scale systems. IEEE Trans Ultrason Ferroelect Freq Contr 1995; 42:429–442.

Kremkau FW. Diagnostic ultrasound: Principles and instruments. Philadelphia: Saunders Elsevier; 2006.

Kremkau FW, Taylor KJW. Artifacts in ultrasound imaging: A review. J Ultrasound Med 1986;5:227–237.

Lockwood GR, Talman JR, Brunke SS. Real-time 3-D ultrasound imaging using sparse synthetic aperture beamforming. IEEE Trans Ultrason Ferroelect Freq Contr 1998;45:980–988.

Nikolov SI, Gammelmark KL, Jensen JA. Recursive ultrasound imaging. Proc IEEE Ultrason Symp 1999;2:1621–1625.

O'Donnell M. Efficient parallel receive beam forming for phased array imaging using phase rotation. Proc IEEE Ultrason Symp 1990;3: 1495–1498.

Ponnle A, Hasegawa H, Kanai H. Multi-element diverging beam from a linear array transducer for transverse cross-sectional imaging of carotid artery: Simulations and phantom vessel validation. Jpn J Appl Phys 2011;50:1–10.

Selesnick IW, Burrus CS. Generalized digital butterworth filter design. Proc IEEE Inter Conf Acoust Speech Signal Proces 1996;3: 1688–1694.

Shattuck DP, Weinshenker MD, Smith SW, von Ram OT. Explososcan: A parallel processing technique for high speed ultrasonic imaging with linear phased arrays. J Acoust Soc Am 1984;75:1273–1282.

Shenoi BA. Introduction to digital signal processing and filter design. Hoboken, NJ: Wiley; 2006.

Shenoi K, Agrawal B. On the design of recursive low-pass digital filters. IEEE Trans Acoust Speech Signal Process 1980;28:79–84.

Smith SW. The scientist and engineer's guide to digital signal processing. San Diego, USA: California Technical Publishing; 1997.

Thomson RN. Transverse and longitudinal resolution of the synthetic aperture focusing technique. Ultrasonics 1984;22:9–15.

Wright JN, Christopher RC, Albert G, Hugh GL, Samuel HM. Method and apparatus for adjustable frequency scanning in ultrasound imaging. US Patent 5549111, 8/1996.

Yamaguchi K, Higashiizumi T, Shimazaki T, Sano S, Takeuchi Y. Azimuth adaptive phased array sonar. US Patent 4631710, 12/1986.